CHARACTERIZING THE EFFECTS OF FRICTION ANGLES ON EARTH PRESSURES IN THE FLOW OF GRANULAR MASS ALONG DOWN-SLOPE AND CROSS-SLOPE IN A ROUGH INCLINE

Jeevan Kafle[1], **Ramuna Pandey**[1], **Bekha Ratna Dangol**[1,2*]

[1]Central Department of Mathematics, Institute of Science and Technology, Tribhuvan University, Kirtipur, Nepal
[2]Department of Mathematics, Patan Multiple Campus, Tribhuvan University, Lalitpur, Nepal
[*]Correspondence: bekha.dangol@pmc.edu.np

ABSTRACT

The tendency of the sliding mass to deform or deposit during the flow strongly depends on the earth pressure coefficient (K) in the dynamics of a finite mass of cohesionless granular material discharged from rest on a rough inclined plane. When the flow velocities along the x and y-axes are decreasing, $K = K_{y\,pas}^{x\,pas}$, the flow becomes convergent, and depositional behavior appears. On the other hand, if the flow velocity is increasing along x-axis but decreasing along y-axis, $K = K_{y\,pas}^{x\,act}$ and the flow is divergent and hence mass spreads. For $K = K_{y\,act}^{x\,pas}$ and $K = K_{y\,act}^{x\,act}$, the flow is neither convergent nor divergent, it remains constant throughout the domain. The mathematical relationship provided here and the associated *2D* and *3D* representation demonstrate how the internal angle (ϕ) and basal angle (δ) of frictions have a significant impact on the earth pressure coefficient in the dynamics of dry granular mass along a rough plane. The mathematical relations for the soil mechanics are also discussed along with these coefficients.

Keywords: Active and passive earth pressures, internal angle of friction, basal angle of friction

INTRODUCTION

Earth pressure problems encountered in engineering practice are concerned with the determination of internal stresses acting on the soil masses or the stresses between the soils and the contiguous structures (Abdul, 1966; Lin *et al.*, 2020). Earth pressure is the lateral force exerted by the backfill on the retaining structures (Kafle *et al.*, 2016; Kafle *et al.*, 2019; Kafle *et al.*, 2023b). The retaining wall frequently pulls away from the backfill as a result of excessive pressure from the retained soil. By resisting forces that are created along the plane of the failure wedge in a direction away from the retaining wall due to the soil's shear strength, the retaining wall is kept in equilibrium (Pirulli *et al.*, 2007; Khosravi *et al.*, 2016; Kafle *et al.*, 2023b). The pressure is limited by the distance that the retaining wall may move from the backfill. Active earth pressure is the least amount of pressure the soil can apply to the retaining wall (Levesque *et al.*, 2017). The earth pressure increases whenever the retaining wall shifts toward the backfill as a result of any natural event because the retaining soil becomes compressed, increasing its shearing strength (Kafle *et al.*, 2023b). When the soil's shearing resistance has fully mobilized, the pressure has reached its maximum level. Passive earth pressure is the maximum earth pressure brought on by the retaining wall's greatest shear stress. Earth pressure at rest is the pressure that forms as a result of backfilling when there is no movement. Its value exceeds limiting active pressure but falls short of passive pressure (Abdul, 1966; Pudasaini & Hutter, 2007; Lin *et al.*, 2020).

The largely unpredictable and devastating natural events like landslides, rockfalls, and snow and ice avalanches occur on steep slopes of mountainous regions that can travel large distances before they come to rest and they frequently pose a threat to human life and their settlements (Kafle *et al.*, 2016; Kafle *et al.*, 2019; Kafle *et al.*, 2022; Kafle *et al.*, 2023a; Kafle *et* *al.*, 2023b). It is extremely challenging and complex to direct observation of the movement of rockfalls or avalanches which is possible only by remote sensing techniques (Gubler, 1987). The study of the dynamics of snow flow avalanches employing radar Doppler techniques was experimented with by Gubler (1987), however it is difficult to study the measurement of the large masses of rocks or soil. Mcfall *et al.* (2018) carried out laboratory experiments dealing with gravel flow to enable the description of the temporal evolution of the front and rear edges as they traveled down a plane surface. Based on continuum mechanics, Savage and Hutter (1989) developed a model to describe the evolving geometry of a finite mass of cohesionless granular material released from rest on a rough inclined plane. The masses of numerous discrete grains initially accelerate quickly downward the slope until the angle of inclination of the bed approaches the horizontal, and bed friction ultimately causes them to come to rest. The granular material is treated as an incompressible Coulomb continuum (Savage & Hutter 1989). Since the sliding of the grains takes place along the bed, the friction angle between the gravel and the rough bed and the internal angle of friction between the grains are actively involved in the model (Hamzah & Omar, 2018).

Numerical simulation can be a helpful tool for examining the propagation phase of phenomena involving granular material, like rock avalanches, when realistic geological contexts are taken into consideration as part of a better territory risk assessment and decision-making process (Faug *et al.*, 2009; Kafle, 2019). Cohesionless granular material free surface gravity-driven flows down a rough inclined plane and overflowing a wall perpendicular to the bottom are examined under steady and erratic incoming flow circumstances (Faug

et al., 2009). The down-slope divergence function $\frac{\partial u}{\partial x}$ is introduced, and its smooth variation and monotonically declining function is used to regularize the down-slope earth pressure coefficient, which approaches the limiting values, $K_{x\,act}$ and $K_{x\,pas}$ for large divergence and convergence respectively. At $\frac{\partial u}{\partial x} = 0$, the down slope earth pressure is at rest (Tai *et al.*, 2001; Pudasaini & Hutter, 2007). A crucial

component of designing passive avalanche defense structures and avalanche hazard zoning is knowing how snow avalanches react to obstacles. Experimental investigations continue to be a crucial method in avalanche science because there isn't a well-established equation that can accurately describe the impact pressure of avalanches on objects of diverse sizes and shapes (Pudasaini & Hutter, 2007; Baroudi *et al.*, 2011).
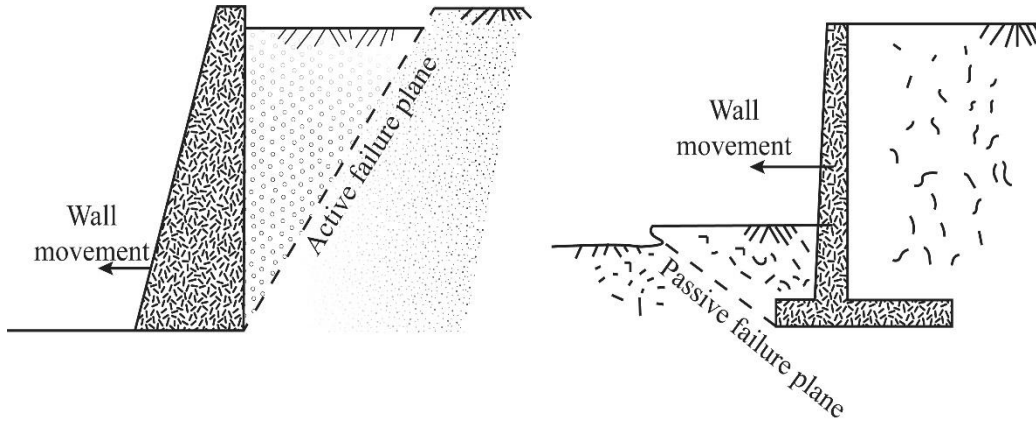
Figure 1. Retaining wall supporting the backfill, Left: Active case where wall moves away from the backfill, Right: Passive case where wall moves towards the backfill (Rankine, 1857)

Coulomb (1776) initially took into account the cohesionless, more flexible mass of dirt moving across a shear surface. By arriving at a solution for an entire soil mass in a failure surface, Rankine (1857) introduced earth pressure. With the aid of the Mohr circle, Rankine analysis was completed. It is usual practice to estimate the active and passive lateral earth pressures using the Rankine theory and the Coulomb theory. Yang and Deng (2019) talked about the implications of backfill width, internal soil friction angle, and wall-soil friction angle in calculating active earth pressure coefficients and classifying them for rigid retaining walls. Levesque et. al. (2017) showed that employing K-values that are calculated as a function of backfill geotechnical characteristics and excavation geometry will increase the precision of the Marston technique for estimating horizontal earth pressure. Mayne *et al.* (2011) discussed coefficient of earth pressure at rest. The numerical simulation makes clear about the significance of adopting a distinct earth pressure coefficient value (K) for the flux's direction of convergence and divergence. Yan *et al.* (2020) determined the distribution of earth pressure by contrasting the impacts of the total active force on the beginning phase, the amplification factor, and the angle of soil friction. The limit equilibrium analysis method is also demonstrated in this study for determining the non-linear distribution of the active earth pressure on stiff retaining walls with constrained backfills (Fig. 1). This study presented the idea that soil deflection plays a more significant role with the narrower width of the backfill and the inclination angle of the triangular failure wedge is connected to the value of the internal friction angle of the solids (Yan *et*

al., 2020). Based on laboratory studies or analytical and numerical models, different researchers proposed various values for the earth pressure coefficient (K). Marston (1930) presented K as the active earth pressure developed by Rankine ($K_a = 0.33$) however Li *et al.* (2009) proposed it as 0.5 to study the deformation of the mass. The properties of the granular material and the roughness of the basal surface specify these coefficients.

The present work demonstrates the characteristics of the earth pressure coefficients in active and passive conditions in different ranges of parameters in both cross-slope and down-slope directions and also varies the ratio of parameters used in the formulation of earth pressure coefficient in the Savage-Hutter model (Savage & Hutter, 1989). Firstly, we discuss the mathematical formulations of the active and passive earth pressure coefficient in Savage-Hutter model for the flow of granular mass in two dimensions. Secondly, we exhibit the reduction of the pressure coefficients in the soil mechanics along cross-slope and down-slope by neglecting the basal angle of friction. Finally, we present some plots to study the variations of the active and passive earth pressure coefficients due to the changes in internal and basal friction angles and their ratios along cross-slope and down-slope directions.

MATHEMATICAL THEORY
An infinitesimal cubic element with a surface perpendicular to the coordinates as extracted from the flowing granular mass. In view of the dominant downward motion, the primary spreading is most probably to occur in the

longitudinal direction, and lateral spreading is almost small. The dominant shearing in the direction parallel to the xz-plane produces the dominant shear stresses τ_{xz} and normal stresses σ_{xx}, σ_{yy}, σ_{zz} as shown in figure 2. Shear stresses τ_{yz} and τ_{xy} also occur but they are significantly smaller than τ_{xz} (Savage & Hutter, 989). It is reasonable to suppose that the lateral confinement pressure σ_{yy} is close to the principal stress say σ_1 because the majority of shearing occurs on vertical surfaces that are parallel to the direction of tangential velocity. The major principal stress is given by (Savage & Hutter, 1989; Kafle *et al.*, 2023b)

$$\sigma_2 = \frac{1}{2}(\sigma_{xx} + \sigma_{zz}) + \frac{1}{2}\sqrt{(\sigma_{xx} - \sigma_{zz})^2 + 4\tau_{xz}^2}$$

and the minor principal stress is given by

$$\sigma_3 = \frac{1}{2}(\sigma_{xx} + \sigma_{zz}) - \frac{1}{2}\sqrt{(\sigma_{xx} - \sigma_{zz})^2 + 4\tau_{xz}^2}$$

The shear stress τ_{xz} and the normal stress σ_{xx} at the bed must be such that they both lie on the wall yield line as indicated in figure 2. It should be noted that two potential Mohr circles can be made through the point corresponding to the stress state meeting the basal sliding law $(\sigma_{xx}^b,\ \tau_{xz}^b)$. According to the usual terminology in soil mechanics, the one corresponding to a higher value of the normal stress is referred to as the passive state of stress, while the other is the active state of stress. We assume that the active or passive state of stress is developed depending on whether an element of granular material is being elongated or compressed in the direction parallel to the bed.

It is assumed that the basal normal stress equals σ_{zz}^b and shear stress equals $-\tau_{xz}^b$. As a result, the basal down-slope normal stress σ_{xx}^b can take on two values, one on the smaller circle $\sigma_{xx}^b \leq \tau_{zz}^b$ and other on the larger circle $\sigma_{xx}^b > \sigma_{zz}^b$ which are associated with active and passive stress states, respectively. The basal cross-slope stress σ_{yy}^b has four possible values since there are four possible values for the major and minor stresses, σ_2^b and σ_3^b. The earth pressure coefficients $K_{x\ act/pas}^b$ and $K_{y\ act/pas}^b$ are defined as follows

$$K_{x\ act/pas}^b = \frac{\sigma_{xx}^b}{\sigma_{zz}^b}, \qquad K_{y\ act/pas}^b = \frac{\sigma_{yy}^b}{\sigma_{zz}^b}$$

In order to establish the value of K_x^b, Savage and Hutter (1989) employed simple arguments, and Hutter *et al.* (1993) used the Mohr-circle representation to define K_y^b as a function of internal (ϕ) and basal angle (δ) of friction, to deduce.

$$K_{x\ act/pas} = 2sec^2\emptyset \left(1 \mp \sqrt{1 - cos^2\emptyset\ sec^2\delta}\right) - 1$$

$$K_{y\ act/pas} = \frac{1}{2}\left[(K_{x\ act/pas} + 1) \mp \sqrt{(K_{x\ act/pas} - 1)^2 + 4tan^2\delta}\right]$$

which are real for $\delta \leq \phi$. The following equation defines the earth pressure coefficient $K_{x\ act/pas}$ as active or passive depending on whether the down-slope motion is dilatational or compressional in order to uniquely calculate the value of the earth pressure coefficient associated with a certain deformation (Savage & Hutter, 1989).

$$K_{x\ act/pas} = \begin{cases} K_{x\ act} & \text{if } \dfrac{\partial u}{\partial x} > 0 \\ K_{x\ pas} & \text{if } \dfrac{\partial u}{\partial x} < 0 \end{cases}$$
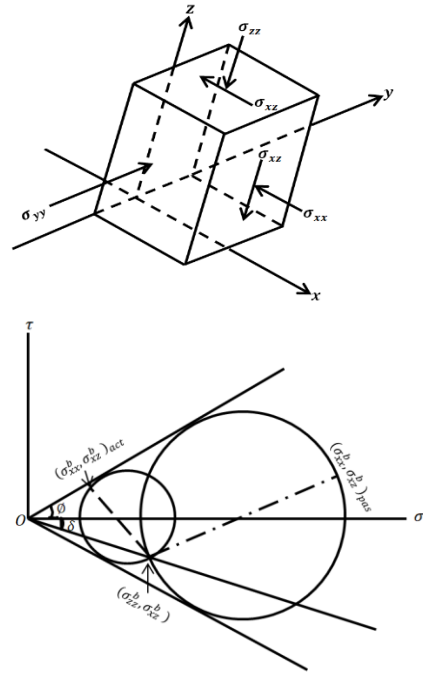
Figure 2. Top: An infinitesimal cubic element with a surface perpendicular to the coordinate axes as extracted from the sliding granular mass. Bottom: Mohr's circle of two-dimensional state of stress representing the relationship between normal and shear stresses (Piruli *et al.,* 2007; Pudasaini & Hutter, 2007)

Comparatively, the dilatational or compressional nature of the down-slope and cross-slope deformation is taken into account when computing the earth pressure coefficients in the lateral direction.

$$K_{y\ act/pas}^{b} = \begin{cases} K_{y\ act}^{x\ act} & \text{if } \dfrac{\partial u}{\partial x} > 0, \dfrac{\partial v}{\partial y} > 0 \\[2mm] K_{y\ pas}^{x\ act} & \text{if } \dfrac{\partial u}{\partial x} > 0, \dfrac{\partial v}{\partial y} < 0 \\[2mm] K_{y\ act}^{x\ pas} & \text{if } \dfrac{\partial u}{\partial x} < 0, \dfrac{\partial v}{\partial y} > 0 \\[2mm] K_{y\ pas}^{x\ pas} & \text{if } \dfrac{\partial u}{\partial x} < 0, \dfrac{\partial v}{\partial y} < 0 \end{cases}$$

The down-slope and cross-slope normal surface stresses at the avalanche's traction-free surface are

$$\sigma_{xx}^{s} = 0, \qquad \sigma_{yy}^{s} = 0$$

Now, intermediate values can be interpolated in accordance with the values of σ_{xx} and σ_{zz} at the base and the free surface. According to the Savage and Hutter theory, through the depth of the avalanche, the down-slope and cross-slope stresses change linearly with normal stress. The following expression accomplishes this. While looking at the rectangular triangle given by the vertices origin, the center of the circle, and the intersection of the circle and tangent, the relation becomes (Pudasaini & Hutter, 2007; Kafle *et al.*, 2023b).

$$r = \frac{r}{\frac{1}{2}(\sigma_{xx} + \sigma_{zz})} \tag{1}$$

Radius of the Mohr circle,

$$r = \sqrt{\tau^2 + \frac{1}{4}(\sigma_{xx} - \sigma_{zz})^2}$$

Substituting the values of τ and r in (1)

$$r = \frac{\sqrt{\sigma_{zz}^2 \tan^2\delta + \frac{1}{4}(\sigma_{xx} - \sigma_{zz})^2}}{\frac{1}{2}(\sigma_{xx} + \sigma_{zz})}$$

Since $K_{x\ act/pas} = \frac{\sigma_{xx}}{\sigma_{zz}}$, squaring both sides then above equation becomes,

$$\frac{1}{4}\sin^2\emptyset \left(K_{x\ act/pas} + 1\right)^2 = \tan^2\delta + \frac{1}{4}\left(K_{x\ act/pas} - 1\right)^2$$

This implies

$$4\tan^2\delta + \left(K_{x\ act/pas}^2 - 2\,K_{x\ act/pas} + 1\right) - \sin^2\emptyset\left(K_{x\ act/pas}^2 + 2\,K_{x\ act/pas} + 1\right) = 0$$

$$4\tan^2\delta + K_{x\ act/pas}^2 \cos^2\emptyset - 2K_{x\ act/pas}(1 + \sin^2\emptyset) + \cos^2\emptyset = 0$$

$$K_{x\ act/pas}^2 - 2\left(\frac{2}{\cos^2\emptyset} - 1\right)K_{x\ act/pas} + 1 + \frac{\tan^2\delta}{\cos^2\emptyset} = 0$$

This is the quadratic equation, its solution is given by

$$K_{x\ act/pas} = \left(\frac{2}{\cos^2\emptyset} - 1\right) \mp \sqrt{\left(\frac{2}{\cos^2\emptyset} - 1\right)^2 - \left(\frac{\tan^2\delta}{\cos^2\emptyset} + 1\right)}$$

$$K_{x\ act/pas} = \left(\frac{2}{\cos^2\emptyset} - 1\right) \mp \sqrt{\frac{4}{\cos^4\emptyset} - \frac{4}{\cos^2\emptyset}(1 + \tan^2\delta)}$$

$$K_{x\ act/pas} = \frac{2}{\cos^2\emptyset}\left(1 \mp \sqrt{1 - \frac{\cos^2\emptyset}{\cos^2\delta}}\right) - 1 \tag{2}$$

Active pressure is denoted by the minus sign, while passive pressure is denoted by the plus sign. In this way $K_{x\ act/pas}$ is depending on the two material constants. In terms of down-slope deformation, $K_{x\ act}$ and $K_{x\ pas}$ represent the extensive and compressive modes, respectively.

In the study of soil mechanics for geotechnical stability, there we ignore the effect of bed friction in relation (2)

$$K_{x\ act/pas} = \frac{2}{\cos^2\emptyset}(1 \mp \sin\emptyset) - 1 \tag{3}$$

If we consider lower sign,

$$K_{pas} = \frac{2(1 + \sin\emptyset) - (1 - \sin^2\emptyset)}{1 - \sin^2\emptyset}$$
$$K_{pas} = \frac{1 + \sin\emptyset}{1 - \sin\emptyset} \tag{4}$$

Also

$$K_{pas} = \frac{1 + \sin\emptyset}{1 - \sin\emptyset} = \left(\frac{1 + \tan^{\emptyset}/_2}{1 - \tan^{\emptyset}/_2}\right)^2$$

We get

$$K_{pas} = \tan^2\left(\frac{\pi}{4} + \frac{\emptyset}{4}\right) \tag{5}$$

Likewise, if we take the upper sign in relation (2)

$$K_{act} = \frac{1 - \sin\emptyset}{1 + \sin\emptyset} = \left(\frac{1 - \tan^{\emptyset}/_2}{1 + \tan^{\emptyset}/_2}\right)^2 \tag{6}$$

Relations $(4), (5)$ and (6) are frequently used in the soil mechanics when stability of the retaining wall against the backfill is analyzed (Marston, 1930). Similarly, for cross-slope the relation is,

$$K_{y\,act/pas} = \frac{1}{2}\left[(K_{x\,act/pas} + 1) \mp \right.$$
$$\left. \sqrt{(K_{x\,act/pas} - 1)^2 + 4tan^2\delta}\right] \quad (7)$$

If we ignore the effect of bed friction angle in relation (7)

$$K_{y\,act/pas} = \frac{1}{2}\{(K_{x\,act/pas} + 1) \mp (K_{x\,act/pas} - 1)\}$$
$$K_{y\,act/pas} = \frac{1}{2}\left\{\frac{2}{cos^2\emptyset}(1 \mp sin\,\emptyset) \right.$$
$$\left. \mp \left(\frac{2}{cos^2\emptyset}(1 \mp sin\emptyset) - 2\right)\right\}$$
$$K_{y\,act/pas} = \frac{1}{cos^2\emptyset}(1 \mp sin\,\emptyset)$$
$$\mp \left(\frac{1}{cos^2\emptyset}(1 \mp sin\emptyset) - 1\right) \quad (8)$$

If we consider positive sign in relation (8), then

$$K_{y\,pas}^{x\,pas} = \frac{2(1 + sin\emptyset)}{cos^2\emptyset} - 1$$
$$= \frac{2(1 + sin\emptyset) - (1 - sin^2\emptyset)}{1 - sin^2\emptyset}$$
$$= \frac{1 + sin\,\emptyset}{1 - sin\,\emptyset} = \left(\frac{1 + tan\,\emptyset/2}{1 - tan\,\emptyset/2}\right)^2$$
$$= tan^2\left(\frac{\pi}{4} + \frac{\emptyset}{4}\right) \quad (9)$$

As we take positive and negative sign respectively in relation (8), then

$$K_{y\,act}^{x\,pas} = \frac{1}{cos^2\emptyset}(1 + sin\,\emptyset) - \left(\frac{1}{cos^2\emptyset}(1 + sin\emptyset) - 1\right)$$
$$= 1 \quad (10)$$

Likewise, if we take negative and positive sign in (8), then

$$K_{y\,pas}^{x\,act} = \frac{1}{cos^2\emptyset}(1 - sin\,\emptyset) + \left(\frac{1}{cos^2\emptyset}(1 - sin\emptyset) - 1\right)$$
$$K_{y\,pas}^{x\,act} = \frac{1}{cos^2\emptyset}(1 - sin\,\emptyset) - 1 = tan^2\left(\frac{\pi}{4} - \frac{\emptyset}{4}\right) \quad (11)$$

And if we take negative sign in (8), then

$$K_{y\,act}^{x\,act} = \frac{1}{cos^2\emptyset}(1 - sin\,\emptyset) - \left(\frac{1}{cos^2\emptyset}(1 - sin\emptyset) - 1\right)$$
$$= 1 \quad (12)$$

Relations $(2), (10), (11)$ and (12) are the cross-slope earth pressure coefficients in the soil mechanics. In relation (10) and (12) we can see the the equation gives the constant value 1 which shows that the longitudinal or lattitudinal pressures and overburden pressure are equal.

RESULTS AND DISCUSSION

To compare the influence of internal friction angle ϕ and bed friction angle δ on the earth pressures along down-slope and cross-slope, we present various two- and three-dimensional plots demonstrating the active and passive earth pressures with regards to the variation in friction of basal surface and /or internal friction angles of grains and their ratios. We describe the material responses in the granular flows in both directions as we mentioned before.

Comparison of effect on the variation of separate friction angles on pressure coefficients along down-slope and cross-slope direction

In the reference graph with the constant bed friction angle 30°, the active and passive earth pressure as a function of the internal angle of friction becomes complex valued when $\delta < \phi$ and the theory becomes invalid in both down-slope and cross-slope. Indeed, there may be a strong shrearing and depth averaging is not adequate. This natural phenomenon is exposed in figures 3A and 3B where the active and passive earth pressure coefficients in both cross-slope and down slope directions have no values for $\phi < \delta = 30^o$. Initially, when $\phi = \delta = 30^o$, both active and passive coefficients are approximately 1.7 in down-slope, whereas $K_{y\,act}$ and $K_{y\,pas}$ along cross-slope are 1.2 and 1.7 respectively. When the internal angle of friction is progressively increased to 60°, active earth pressure coefficient along down-slope decreases from 1.7 to 0.4 while passive coefficient increases sharply from 1.7 to 13.5. Regarding along the cross-slope, $K_{y\,act}^{x\,act}$ and $K_{y\,pas}^{x\,pas}$ slightly decreases whereas $K_{y\,act}^{x\,pas}$ increases slightly. On the contrary, $K_{y\,act}^{x\,pas}$ $K_{y\,pas}^{x\,act}$ sharply increases from 1.7 to 13.5. The earth pressure depending on both directions is relatively more realistic than that depending on only one direction as dry granular mass advects not only in the down-slope but also disperses along cross-slope.

$K_{y\,pas}^{x\,pas}$ increases sharply when when ϕ exceeds 45° as the coarse particle with greater internal friction angle of the grain increases the resisting force to bear the destabilizing force (normal stress). In this situation, the passive earth pressure is smooth along the cross-slope direction. This demonstrate that the internal friction angle has major influence on the passive earth pressure coefficient, but it has negligible influence on $K_{y\,pas}^{x\,act}$ and $K_{y\,act}^{x\,pas}$ however moderate influence on the active earth pressure coefficients. This is due to the fact that as the internal friction angle decreases, the lateral shearing stress of the material also decreases, making the granular mass more extensive along both down-slope and cross-slope. Proximity of both friction angles results in the

closer values of both earth pressure coefficients in granular mass.
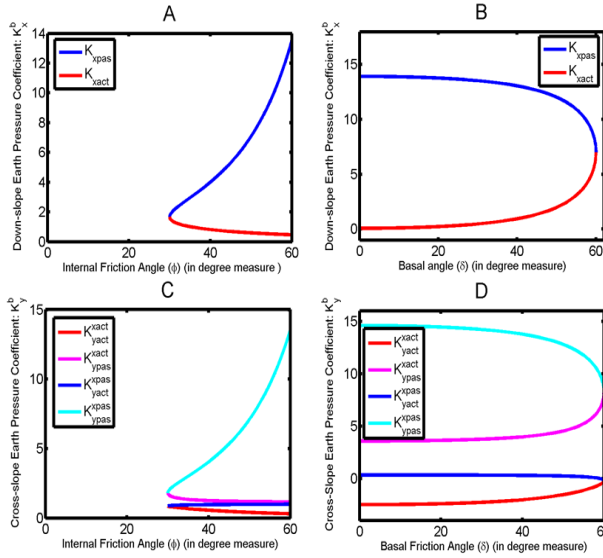
Figure 3. Active and passive earth pressures along A) down slope and C) cross-slope with the variation in internal friction angle with constant basal angle of friction as 30° and B) down slope and D) cross-slope with the change in bed friction angle with constant angle of internal friction as 60°

Figures 3B and 3D exhibit the graph of the active and passive pressure coefficients depending on the bed friction angles while the internal friction angle of the grains is assumed to be constant as $\phi = 60^o$. Firstly, when basal friction angle $\delta = 0^o$, the active and passive earth pressure coefficient are 0 and 13.9 in down-slope respectively however they are 0.07 and 13.9 along cross-slope respectively. As δ increases, $K_{x\,pas}$ decreases from 13.9 to 7, and $K_{x\,act}$ increases to 7 whereas $K_y^{x\,pas}$ decreases from 13.9 to 7 and $K_y^{x\,act}$ increases smoothly from 4 to 7 and $K_y^{x\,act}$ decreases smoothly from 0.1 to 0.

The evolution of the pressure coefficients in figures 3B and 3D are reverse in comparison to that in figures 3A and 3C. When there is a significant difference between the friction angles, the active and passive coefficients diverge significantly from one another. The active and passive earth coefficients become closer in accordance with the increasing proximity of the friction angles and hence $K_{x\,act} = K_{x\,pas}$, $K_y^{x\,act} = K_y^{x\,pas}$, $K_y^{x\,act} = K_y^{x\,pas}$ when $\delta = \phi$. Additionally, we can observe that when δ varies from 0° to 45°, $K_{x\,pas}$ and $K_y^{x\,pas}$ decreases marginally while $K_{x\,act}$ and $K_y^{x\,act}$ gradually increases. On the contrary, when δ exceeds 45°, $K_{x\,pas}$ and $K_y^{x\,pas}$ both decline rapidly but $K_{x\,act}$ increases rapidly while $K_y^{x\,act}$ increases slowly. It depicts that the increment of the roughness of the inclined plane tends the flow more compressive rather than extensive. Both the earth pressures changes abruptly when δ exceeds 45° and similar behavior

can be observed in figure 3(A) when $\phi > 45^o$. However, $K_y^{x\,act}$ has no substantial shift in its graph as compared to the active earth pressure in down slope, it concludes that active coefficient changes abruptly along down-slope direction rather than in cross-slope direction.

Also, from the results, we can conclude that the value of K is consistent if the values of δ and ϕ are close to each other. The further values of K can not be obtained when δ exceeds 60°. In figures 3A, 3C and figures 3B, 3D, we observe that $K_{x\,pas} \geq K_{x\,act}$ and $K_y^{x\,pas} \geq K_y^{x\,act}$. That is passive earth coefficient is always greater than or equal to the active pressure coefficient along both down-slope and cross-slope direction.

Comparison between the earth pressure coefficients against internal friction angle for different ratios of basal to internal friction angles along cross- and down-slope direction

The variation and proximity of the friction angles are very common material properties of the various granular mass. Now, we discuss the proportional effects on the earth pressures along longitudinal and lateral directions. For this purpose, we vary the ratio of these friction angles, and induced longitudinal and lateral pressure coefficients are plotted in figure 4.

Figure 4A shows the graph of active pressure coefficients as a function of internal friction angle for three different ratios of δ and ϕ. As $\frac{\delta}{\emptyset} = 1$, K_{act} increases from 1 to 7, whereas it decreases from 1 to 0.47, and from 1 to 0.07 when $\frac{\delta}{\emptyset} = 0.5$ and $\frac{\delta}{\emptyset} = 0$ respectively. Instead, the value of the coefficient is the least if the internal angle of friction is much larger than that of bed. For $\frac{\delta}{\emptyset} = 1$, value of K_{act} increases more rapidly for values of ϕ higher than 45°. On contrary, it decreases significantly when $\phi < 45^o$, in case if $\frac{\delta}{\emptyset} = 0.5$ and $\frac{\delta}{\emptyset} = 0$. So, $\phi = 45^o$ is somehow behaves as a critical friction angle. There is not much larger difference in the values of K_{act} when the ratio $\frac{\delta}{\emptyset} \leq 0.5$. It is equally interesting to observe that K_{act} is increasing when $\frac{\delta}{\emptyset} = 1$, i.e., for $\delta = \phi$ but slowly decreases when $\frac{\delta}{\emptyset} = 0.5$, i.e., $\delta = \frac{1}{2}\phi$ and rapidly decreases for $\frac{\delta}{\emptyset} = 0$, i.e., $\delta = 0$.

For different ratios of δ and ϕ, figure 4B represents the graph of passive earth pressure coefficients against internal friction angles. As $\frac{\delta}{\emptyset} = 1$, K_{pas} increases from 1 to 7 which is the same graph of K_{act} as in figure 4A. It means that active and passive pressure coefficients are both equal when $\phi = \delta$. When $\frac{\delta}{\emptyset} = 0.5$, K_{pas} increases from 1 to 13.5. In similar

manner, it increases from 1 to 13.9 when $\frac{\delta}{\phi} = 0$. Like the active pressure, K_{pas} also has a smaller deviation when $\frac{\delta}{\phi} \leq \frac{1}{2}$. As the ratio of basal angle and internal angle of friction decreases, the active pressure decreases but the passive pressure increases. When ϕ exceeds 45°, the pressure coefficients change significantly.
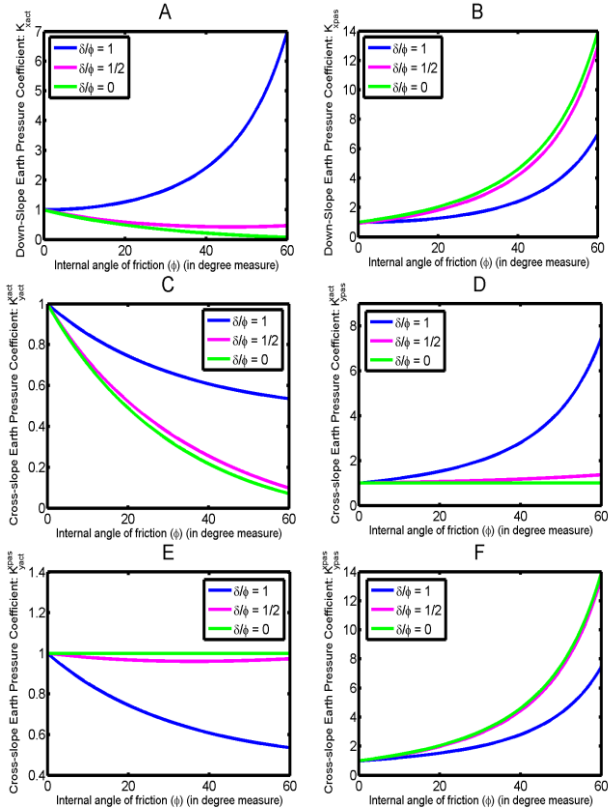
Figure 4. Down-slopes of: A) Active and B) Passive earth pressure coefficients and cross-slopes of C) $K_{y\,act}^{x\,act}$, D) $K_{y\,pas}^{x\,act}$, E) $K_{y\,act}^{x\,pas}$ and F) $K_{y\,pas}^{x\,pas}$ due to the variation in internal friction angle with constant basal angle of friction as 30°

On the other hand, figure 4C shows $K_{y\,act}^{x\,act}$ as a function of the internal friction angle for the aforementioned ratio. As $\frac{\delta}{\phi} = 1, K_{act}$ increases from 1 to 7, whereas it decreases from 1 to 0.47 and from 1 to 0.07 when $\frac{\delta}{\phi} = \frac{1}{2}$ and $\frac{\delta}{\phi} = 0$ respectively along down-slope. The same thing takes place in cross-slope direction as $\frac{\delta}{\phi} = 1$, $K_{y\,act}^{x\,act}$ decreases from 1 to 0.57, whereas it decreases from 1 to 0.05 and from 1 to 0.04 when $\frac{\delta}{\phi} = \frac{1}{2}$ and $\frac{\delta}{\phi} = 0$, respectively. It means that if the velocity gradient is positive, the flow is highly extensive whenever ϕ and δ are higher and equal. But if the velocity gradient is positive in both initial and final state, the flow is slightly compressive. On contrary, it decreases significantly when $\phi < 45^o$ in case of cross-slope it continues down to

decreasing. But in case of cross-slope in figure 4D, as $\frac{\delta}{\phi} = 1$, $K_{y\,act}^{x\,act}$ increases from 1 to 7.5 whereas it increases 1 to 1.5 for $\frac{\delta}{\phi} = \frac{1}{2}$ and it remains constant throughout the domain and for $\frac{\delta}{\phi} = \frac{1}{2}$, it decreases from 1 to 0.95 and as $\frac{\delta}{\phi} = 1$, it decreases from 1 to 0.05. As the ratio of the basal and internal angle of friction decreases, the active earth pressure also decreases but passive earth pressure increases along the down-slope. On the other hand, $K_{y\,act}^{x\,act}$ and $K_{y\,pas}^{x\,act}$ decreases but $K_{y\,pas}^{x\,pas}$ and $K_{y\,act}^{x\,pas}$ increases when ϕ exceeds 40°.

Comparison between changes in coefficients against basal friction angle for different ratios of friction angles along down-slope and cross-slope

Earth pressure coefficients depend on the basal angle of friction. By considering different ratios of friction angles, figure 5 illustrates the active and passive earth pressure coefficients as a function of bed friction angle along down-slope and cross-slope. Figures 5A and 5B are the evaluation of active and passive earth pressure coefficients for different values of basal friction angles along down-slope and figures 5C-F are the evaluations of earth pressure coefficients along cross-slope.

As $\delta = \phi$, active earth pressure is increases from 1 to 1.7, passive earth pressure is increases from 1 to 10 till the bed angle is 25°. After exceeding 25°, it increases rapidly along down slope. The earth pressure coefficient $K_{y\,act}^{x\,act}$ decreases from 1 to 0.67 and whereas $K_{y\,pas}^{x\,act}$ increases from 1 to 2 and $K_{y\,act}^{x\,pas}$ decreases from 1 to 0.7 and $K_{y\,pas}^{x\,pas}$ increases from 1 to 1.5. In contrast, active earth pressure decrease from 1 to 0.73 and 1 to 0.48 when $\frac{\delta}{\phi} = \frac{3}{4}$ and $\delta\frac{\delta}{\phi} = \frac{1}{2}$ respectively along down slope, and passive earth pressure, increases from 1 to 4 and 1 to 2 when $\frac{\delta}{\phi} = \frac{3}{4}$ and $\frac{\delta}{\phi} = \frac{1}{2}$ along cross-slope respectively. We clearly observe that active earth pressure in figure 4A is much higher than figure 5A. So, we conclude that the influence of internal friction angle (ϕ) is higher than the basal friction angle (δ) for the variation of active earth pressure K_{act} along both directions. Active earth pressure decreases as internal friction angle increases relative to the basal friction angle. But K_{pas} shows completely opposite behavior that can be seen in the figure 5B in down-slope. In different circumstances $K_{y\,act}^{x\,pas}$ decreases as the increasing basal angle. But $K_{y\,pas}^{x\,pas}$ show the complete opposite behavior that can be seen in figure 5F. The pressure coefficients at various basal friction angles are significantly affected by the inclusion of cross-slope and down-slope directions. In a real-world setting, cross-slope and down-slope have an impact on each other's earth pressure.
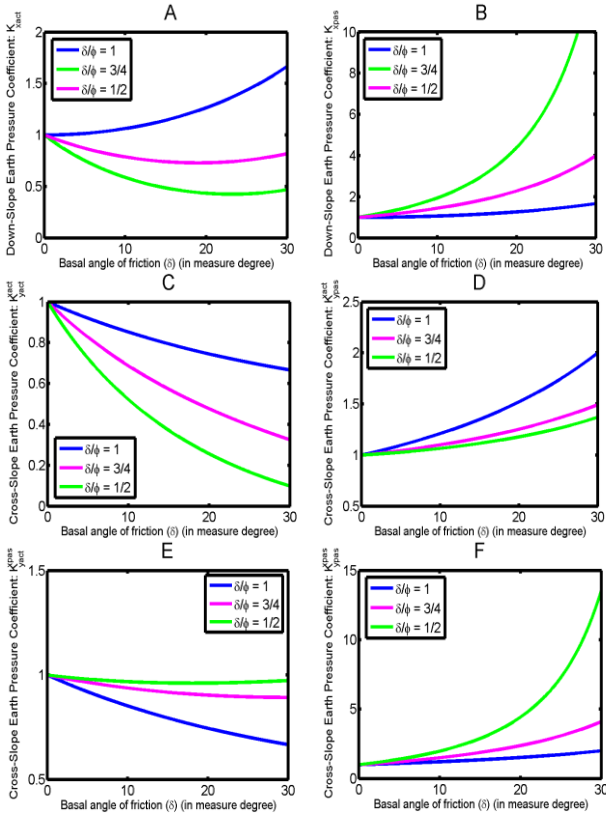
Figure 5. Down-slopes of: A) Active and B) Passive earth pressure coefficients and cross-slopes of C) $K_{y\,act}^{x\,act}$, D) $K_{y\,pas}^{x\,act}$, E) $K_{y\,act}^{x\,pas}$ and F) $K_{y\,pas}^{x\,pas}$ due to the variation in basal friction angle with constant internal angle of friction as 30°

Figure 6. Down-slopes of: A) Active and B) Passive earth pressure coefficients and cross-slopes of C) $K_{y\,act}^{x\,act}$, D) $K_{y\,pas}^{x\,act}$, E) $K_{y\,act}^{x\,pas}$ and F) $K_{y\,pas}^{x\,pas}$ due to the 3-D variation in internal friction angle and basal angle of friction

Comparison between earth pressure coefficients as functions of both angles of basal and internal friction along down and cross-slope

The values of the earth pressure coefficients as a function of both basal angle and internal angle of friction is represented in 3-D graph along down-slope and cross-slope direction. Two-dimensional graph revealed that K_{act} is maximum when $\delta = \phi$, and this result can also be seen in figure 6A within the entire domain $0 \le \phi \le 60^o$, $0 \le \delta \le 60^o$, maximum of K_{act} is 7 when $\delta = \phi = 60^o$. Similarly, the maximum value of K_{pas} is 14 at $\delta = 0^o$, $\phi = 60^o$ and minimum value is 1 at $\delta = \phi = 0^o$ which can also be observed in figure 6B along down-slope. In a similar manner $K_{y\,act}^{x\,act}$ is maximum at 1 and minimum at 0 within the domain $0 \le \phi \le 50^o$, $0 \le \delta \le 50^o$, $K_{y\,pas}^{x\,act}$ is maximum at 7 and minimum at 1 within the domain $0 \le \phi \le 50^o$, $0 \le \delta \le 60^o$, $K_{y\,act}^{x\,pas}$ is maximum at 1 and minimum at 0 within the domain $0 \le \phi \le 50^o$, $0 \le \delta \le 50^o$, $K_{y\,pas}^{x\,pas}$ is maximum at 14 and minimum at $\delta = 0^o$, $\phi = 60^o$ and minimum value is at 1 at $\delta = \phi = 0^o$ which is observed in figure 6F.

Comparison between earth pressure in soil mechanics along down and cross-slope

The ratio of horizontal stress to vertical stress in soil mechanics is the earth pressure coefficient. In figure 7A, K_{act} becomes less than 1 as the vertical stress dominates the horizontal stress, and as ϕ increases K_{act} decreases, K_{pas} increases, $K_{y\,act}^{x\,act}$ decreases, $K_{y\,pas}^{x\,act}$ decreases, $K_{y\,act}^{x\,pas}$ increases and $K_{y\,pas}^{x\,pas}$ increases because a higher internal friction angle makes the soil more compressive.
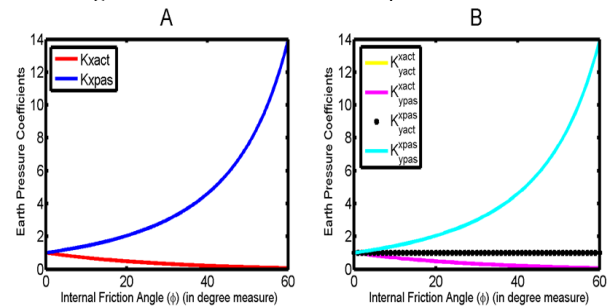
Figure 7. A) Earth pressure coefficients along down-slope B) Earth pressure coefficients along cross-slope

CONCLUSIONS

The gravity driven dry granular materials advects not only in the down-slope, but also disperses along cross-slope. So, the study of earth pressure coefficients along both directions is essential and realistic. Normally, active earth pressure coefficients refer that the flow divergent affecting the larger area whereas the passive earth pressure coefficient describes that the flow is convergent affecting the smaller area in the sliding zone. If the basal friction angle exceeds the internal friction angle, the flow will have large spreading and hence depth average will not be adequate for numerical modeling. The earth pressure coefficient is an isotropic pressure coefficient if there is no internal friction angle or basal friction angle. Initially, when the basal angle is fixed at 60^0 the earth pressure has no effect till $\phi < 30^0$, in both cross-slope and down slope direction but after the internal angle reaches the passive earth pressure increases drastically up to 13.9 and the active earth pressure decreases smoothly within the domain $0 \leq \phi \leq 60^0$. Similarly taking the internal angle fixed at 60°, the passive earth pressure decreases down to 7 along both cross-slope and down-slope direction. The substantial increment or decline in the earth pressure coefficients are studied in the vicinity of 45^0 of internal friction angle. So, 45^0 is the critical angle of internal friction. We can conclude that the passive earth pressure coefficients vary directly with the internal angle of friction and inversely with the basal angle of friction along both directions.

ACKNOWLEDGEMENTS

AUTHORS CONTRIBUTION STATEMENT

JK: Developed the idea, designed the research work and edited the manuscript; RP: designed the research plan and wrote the manuscript; BRD: Organized the study and contributed to results and discussion.

CONFLICT OF INTEREST

The authors do not have any conflict of interest pertinent to this work.

DATA AVAILABILITY STATEMENT

The data that support the findings of this study are available from the corresponding author, upon reasonable request.

REFERENCES

Abdul, A.F. (1966). *A Direct method for the determination of earth pressures on retaining walls*, Ph.D. Thesis, Oklahoma State University Stillwater, Oklahoma.

Baroudi, D., Sovilla, B., & Thibert E. (2011). Effects of flow regime and sensor geometry on snow avalanche impact-pressure measurements. *Journal of Glaciology*, *57*(202), 277-288.

Coulomb, C.A. (1776). An attempt to apply the rules of maxima and minima to several problems of stability related to architecture. *M´emoires l'Acad´emie, Royale Des Sciences*, 343–382.

Faug, T., Beguin, R., & Chanut, B. (2009). Mean steady granular force on a wall overflowed by free-surface gravity-driven dense flows. *Physical Review E*, *80*, 021305.

Gubler, H.U. (1987). Measurements and modelling of snow avalanche speeds. *Avalanche Farmation, Movement and Effects, 126*, 405-420.

Hamzah, M.B.A., & Omar S.B.A. (2018). A review on the angle of repose of granular materials. *Powder Technology, 330,* 397-417.

Hutter, K., Siegel, M., & Savage, S.B. (1993). Two-dimensional spreading of a granular avalanche down an inclined plane Part I. theory. *Acta Mechanica*, *100,* 37–68 .

Kafle, J., Pokhrel, P.R., Khattri, K.B., Kattel, P., Tuladhar, B.M., &Pudasaini, S.P. (2016). Landslide-generated tsunami and particle transport in mountain lakes, reservoirs. *Annals of Glaciology, 57*(71), 232-244.

Kattel, P., Kafle, J., Fischer, J.-T., Mergili, M., Tuladhar, B.M., & Pudasaini, S.P. (2018). Interaction of two-phase debris flow with obstacles. *Engineering Geology*, *242*, 197-217.

Kafle, J., Kattel, P., Mergili, M., Fischer, J.-T., & Pudasaini, S.P. (2019). Dynamic response of submarine obstacles to two-phase landslide and tsunami impact on reservoirs. *Acta Mechanica*, *230*(9), 3143-3169.

Kafle, J., Acharya, G., Kattel, P., & Pokhrel, P.R. (2022). Impact of variation of size of the initial release mass in the dynamics of landslide generated tsunami. *International Journal of Modeling, Simulation, and Scientific Computing*, *13*(5), 217-225.

Kafle, J., Dangol, B.R., Tiwari, C.N., & Kattel, P. (2023a). Dynamics of landslide-generated tsunamis and their dependence on the particle concentration of initial release mass. *European Journal of Mechanics - B/Fluids, 97*, 146-161.

Kafle, J., Pandey, R., Dangol, B.R., Tiwari, C.N., & Kattel, P. (2023b). Influence of friction angles on earth pressures in dry granular flow dynamics and soil mechanics. *The Nepali Mathematical Sciences Report*, *39*(2), 25-37.

Khosravi, M.H., Pipatpongsa, T., & Takemura, J. (2016). Theoretical analysis of earth pressure against rigid retaining walls under translation mode. *Soils and Foundations,* 56(4), 664-675.

Levesque, Y., Saeidi, A., & Rouleau, A. (2017). An earth pressure coefficient based on the geomechanical and geometric parameters of backfill in a mine stope. *Geo-Engineering*, *27*(8), 1-15.

Li, L., & Aubertin, M., (2009) Numerical investigation of the stress state in inclined backflled stopes. *International Journal of Geomechanics*, *27*, 52–62.

Lin, Y., Chen, F., Yang, J., & Li, D. (2020). Active Earth Pressure of Narrow Cohesionless Backfill on Inclined Rigid Retaining Walls Rotating about the Bottom. *International Journal of Geomechanics*, *20*(7), 04020102. https://doi.org/10.1061/(asce)gm.1943-5622.0001727.

Marston, A. (1930). The theory of external loads on closed conduits in the light of the latest experiments. *Proceedings of the Nineth Annual Meeting of the Highway Research Board,* Washington, D.C., December 12-13. 1929.

Mayne, P., & Kulhawy, F. (2011). The coefficient of earth pressure at rest. *Canadian Geotechnical Journal, 31*, 788-790.

Mcfall, B., Mohammed, F., Fritz, H., & Liu, Y. (2018). Laboratory experiments on three dimensional deformable granular landslides on planar and conical slopes. *Landslides*, *15*(12), 1713-1730. https://doi.org/10.1007/s 10346-018-0984-2.

Pirulli, M., Bristeau, M.O., Mangeney, A., & Scavia, C. (2007). The effect of the earth pressure coefficients on the runout of granular material, *Environmental Modelling and Software*, *22*, 1437-1454.

Pudasaini, S.P., & Hutter, K. (2007). *Avalanche dynamics: Dynamics of rapid flows of dense granular avalanches*. Springer.

Rankine, W.J.M. (1857). On the stability of loose earth. *Philosophical Transactions of the Royal Society of London, 147*, 9–27.

Savage, S.B. & Hutter, K. (1989). The motion of a finite mass of granular material down a rough incline. *Journal of Fluid Mechanics*, *199*, 177-215.

Tai, Y.C., Hutter, C., & Gray, J. (2001). Dense granular avalanches: Mathematical description and experimental validation. *Geomorphological Fluid Mechanics, 582*, 339-366.

Yan, Z., Deng, Y., He, J., Xuan, Y., & Wu, W. (2020). A pseudodynamic approach of seismic active pressure on retaining walls based on a curved rupture surface. *Mathematical Problems in Engineering*, *5*, 1-8.

Yang, M., & Deng, B. (2019). Simplified method for calculating the active earth pressure on retaining walls of narrow backfill width based on DEM analysis. *Advances in Civil Engineering*, *2*, 1-12.